REPORT DOCUMENTATION PAGE

Form Approved
OMB No. 0704-0188

1. REPORT DATE *(DD-MM-YYYY)*	**2. REPORT TYPE**	**3. DATES COVERED** *(From - To)*
29-02-2012	FINAL	From 4/1/2008 to 11/30/2011

4. TITLE AND SUBTITLE

Computational Nanotribology of Nanometer Confined Liquid Films

5a. CONTRACT NUMBER

5b. GRANT NUMBER
FA9550-08-1-0214

5c. PROGRAM ELEMENT NUMBER

6. AUTHOR(S)

Yongsheng Leng & Peter T. Cummings

5d. PROJECT NUMBER

5e. TASK NUMBER

5f. WORK UNIT NUMBER

7. PERFORMING ORGANIZATION NAME(S) AND ADDRESS(ES)

Vanderbilt University, Dept. Chemical & Biomolecular Eng.
Nashville, Tennessee 37235

George Washington University,
Dept. Mechanical & Aerospace
Eng., Washington, DC 20052

8. PERFORMING ORGANIZATION REPORT NUMBER

9. SPONSORING / MONITORING AGENCY NAME(S) AND ADDRESS(ES)

Joycelyn Harrison
AFOSR/RSA
875 North Randolph Street
Suite 325, RM 3112
Arlington, VA 22203

10. SPONSOR/MONITOR'S ACRONYM(S)

11. SPONSOR/MONITOR'S REPORT NUMBER(S)
AFRL-OSR-VA-TR-2012-1140

12. DISTRIBUTION / AVAILABILITY STATEMENT

Distribution A: Approved for Public Release

13. SUPPLEMENTARY NOTES

14. ABSTRACT

The authors have performed extensive computational molecular dynamics simulations to study the structure and dynamics of nanometer confined liquid films between solid surfaces. A specific computational tool, namely, the liquid-vapor molecular dynamics (LVMD) was developed. They revealed repulsive hydration force mechanism and load bearing capacity of aqueous electrolytes between two charged surfaces. They also studied the force oscillation and liquid-to-solid phase transition mechanisms of nonpolar simple fluids under confinement. A new principle of stick-slip friction and energy dissipation mechanism was also developed through this project.

15. SUBJECT TERMS

16. SECURITY CLASSIFICATION OF:			**17. LIMITATION OF ABSTRACT**	**18. NUMBER OF PAGES**	**19a. NAME OF RESPONSIBLE PERSON**
a. REPORT	**b. ABSTRACT**	**c. THIS PAGE**			**19b. TELEPHONE NUMBER** *(include area code)*

Final Report for
AFOSR Award No. FA9550-08-1-0214

Computational Nanotribology of Nanometer Confined Liquid Films

February 29, 2012

Principal Investigators:

Yongsheng Leng
Department of Mechanical & Aerospace Engineering
The George Washington University
Washington, DC 20052
Tel: 202-994-5964
Email: leng@gwu.edu

And

Peter T. Cummings
Department of Chemical & Biomolecular Engineering
Vanderbilt University
Nashville, Tennessee 37235
Tel: 615-322-8129
Email: peter.cummings@vanderbilt.edu

Program Manager:
Joycelyn Harrison, Ph. D.
AFOSR Program Manager
Surface and Interfacial Science and Low Density Materials
875 North Randolph St.
Suite 325, Room 3112
Arlington, VA 22203

Research objectives:

Normal forces between two solid surfaces in liquids, namely, the solvation forces, are closely related to the structure and dynamic properties of nanometer confined liquid films. The associated fundamental questions are of central importance in a broad spectrum of disciplines, such as materials science, microfabrication, micro/nano electro-mechanical systems (M/NEMS) design, colloidal science, geology, and biological lubrication in soft matter biology. In the field of nanotribology, particularly in the surface force apparatus (SFA) experimental community, there are long-standing debates regarding the thermodynamic state of nanoconfined fluids and the nature of their shear properties. The goals of this AFOSR project are: (1) to develop a computational approach incorporating realistic molecular models and simulation ensembles to investigate, at a molecular level, the inherent force laws in nanoconfined liquids; (2) For aqueous system, to understand the underlying mechanism of repulsive hydration force between charged surfaces in pure water and aqueous electrolyte solutions; and (3) for nonpolar liquid system, to understand the origin of oscillatory behavior of solvation forces and the ordering and packing structures of different non-polar liquids with different architectures. (4) The stick-slip friction and energy dissipation in boundary lubrication. The outcomes of this research project advance the development of enabling-technologies in nanotribology and MEMS/NEMS devices, which is a key component of current Air Force Research in terrestrial surveillance applications.

Significant work accomplished:

1. Development of the liquid-vapor molecular dynamics (LVMD) simulation method

Liquid film confined between two solid surfaces is a strongly inhomogeneous system. The pressure parallel to the confining wall is quite different from the normal pressure due to the formation of layered structures. In surface force experiments, the equilibrium between the confined and the bulk fluids requires that the chemical potentials in these two regions should be equal. One way to represent the connection between the confined and bulk fluids is to use the so-called isothermal-isostress ensemble, in which the lateral pressures are controlled to the desired bulk values. The grand canonical ensemble was also designed for this purpose. However, for a two-dimensional (2D) confined system, particularly when explicit surface atoms and charges are present, the calculation of pressure tensor is a nontrivial issue.

We note that in surface force experiments, the ambient condition requires that the bulk liquid pressure should be close to 1 *atm*. This is a vanishingly low pressure compared to the thermal fluctuations of internal pressures in liquids. For this reason, two liquid-vapor interfaces are introduced around the confined liquid phase, resulting in the lateral pressure comparable to the vapor pressure. This treatment avoids the scaling of the particle coordinates to control the pressure. Consequently, molecular trajectories of liquid will not be disrupted. In the LVMD simulation, a simple driving spring model is applied to mimic the force measurement in surface force experiments. The main features of simulation method are shown in Fig. 1 (a). A liquid droplet is introduced between two solid walls. The coexistence of two vapor phases around the central liquid droplet allows for the squeeze out of the fluid to proceed naturally. At the same time the lateral pressure

is maintained at vanishingly low value. Normal approach and retraction are carefully controlled by moving the upper confining wall that follows a rigid-body driven dynamics motion (Fig. 1A). Each confining wall is composed of a central wall that has realistic atomic interactions with the fluid while the side walls only apply unidirectional constraint to liquid molecules. Consequently, in LVMD, only the forces acting on the discrete atoms of the top central wall are counted towards the total normal force. In this way, when the liquid droplet is squeezed out sufficiently, meniscus effect will have minimal effect on the forces between two central walls. Figure 1(b) shows a liquid argon droplet confined between to solid crystals, in which both the liquid and vapor phases are quite stable.

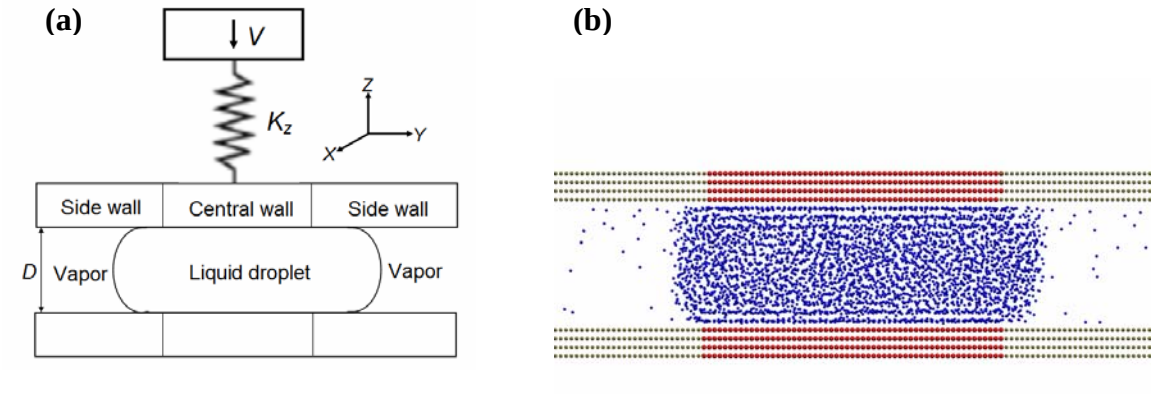

Figure 1. (a) Sketch of the liquid-vapor molecular dynamics (LVMD) model; (b) Argon droplet confined between two crystalline walls.

2. Origin of the repulsive hydration force between two charged mica surfaces in electrolytes

Over thirty years ago, Israelachvili and Adam [J. Chem. Soc. - *Faraday Transactions* (1978)] and later Israelachvili and Pashley [*Nature* (1983); *J. Colloid Interface Sci.* (1984)] investigated the normal forces between two mica sheets in aqueous electrolyte solutions. In dilute electrolytes or acid solutions, the variation of the surface force versus mica gap distance follows the Derjaguin-Landau-Verwey-Overbeek (DLVO) theoretical prediction, which states that the mutual repulsion between two mica surfaces at a large distance and attractive collapse at a distance of a few nanometers are associated with the force balance between the electrostatic repulsive double-layer force and van der Waals attractive force. In very dense electrolytes, however, an additional strong repulsive force at short distances (particularly, in a distance less than a few nm), namely *hydration force*, prevents van der Waals attractive collapse between two mica surfaces. However, explanations to the physics of this hydration force are still quite controversial. It has been claimed that either the anomalous dielectric response of water near charged surfaces, or the effect of dielectric overscreening in electrostatics for water, was responsible for the short-range repulsion. This is in contrast to the argument that water should not have a different dielectric constant near or between two surfaces.

The LVMD simulations were performed to study the load-bearing capacity of 1M KCl solution. Figure 2 shows the force profile during normal compression versus the distance between two mica surfaces. Repulsive hydration force is seen in the range of D =

0.75 – 1.99 nm, where the force magnitude in the range of 0 – 10nN. The force increases sharply when D < 1.0 nm. This repulsive hydration force is much stronger than the continuum double-layer electrostatic force (see Fig. 2). Moreover, the repulsive force is not monotonic, but has a step-like oscillatory feature in the range of D = 1.09 – 2.13 nm. The exponential decay length is estimated around 0.28 nm, close to the Debye length of the double-layer force in 1M KCl electrolyte, as well as the diameter of water molecules. This force oscillatory behavior is very similar to what was observed in the SFA experiment by Pashley and Israelachvili (1984). However, more force oscillations were found in the experiment (the green line) due to the mica-glue deformation in SFA.

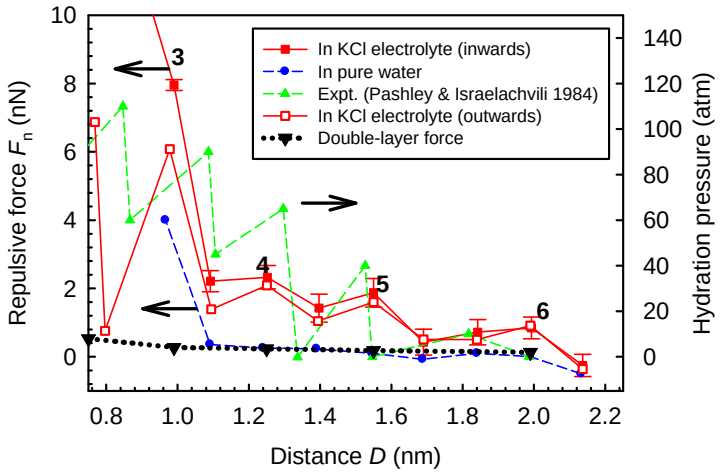

Figure 2. Repulsive hydration force profile between two mica surfaces in 1M KCl electrolyte solution. The numerical numbers 6, 5, 4, and 3 represent different layers of hydration film. Experimental hydration pressures (green triangle, in the unit of MPa on the right axis) and continuum double-layer forces (black triangle) are also shown for comparison. Forces in pure water (blue) are also shown for comparison. Error bars indicate the force variance.

To verify that the strong repulsive hydration force is indeed related to the hydrated K^+ ions and Cl^- co-ions in KCl electrolyte, we recalculated the forces between the two mica surfaces in pure water, by simply removing the 34 K^+ ions and 34 Cl^- co-ions in the aqueous film. In this case, as shown in Figure 2, the overall magnitude of the force between two mica surfaces in pure water (the blue line) is much smaller than those in 1M KCl electrolyte. The strong repulsive force at D < 1 nm in pure water is simply because of the overlaps of the adsorbed K^+ hydration shells near mica surfaces.

The corresponding equilibrium molecular configurations and density distributions of water O, K^+ ions, and Cl^- co-ions at 6 to 2 different hydration layers (the layer thickness varies from 1.99 nm to 0.75 nm) are shown in Fig. 3, where both K^+ and Cl^- have distinct peaks at different locations. Further diffusion calculations for water, K^+ and Cl^- different species show that they all have significant diffusions even under extreme confinement. Compared with the diffusion constant of bulk water, the decrease in diffusion of these species under confinement is no more than three orders of magnitude.

The origin of the strong repulsive hydration force of nanoconfined electrolyte has been further studied through the investigation of the hydration shell structures of K^+ ions and Cl^- co-ions. The most significant finding is the distinction between the ion-water and

anion-water pair correlation functions (Fig. 4), which strongly suggests that there exist a "hard" K^+ and a "soft" Cl^- hydration shells — As the degree of confinement increases from D = 1.99 nm to D = 0.75 nm, the radius of K^+ 1st hydration shell essentially has no change, and its 2nd hydration shells has an inward shift of 0.25 Å (or ~5% of the second hydration radius) only at the D = 0.99 nm film thickness. In contrast, the radii of Cl^- hydration shells change dramatically, especially the second hydration shell of Cl^- co-ions shrinks by ~ 1 Å, or by ~ 21% relative to $r_{2\text{-}Cl}$ = 4.85Å. Consequently, the load bearing capacity of dense electrolyte under nanometers confinement is largely attributed to the critical role of hydrated metal ions.

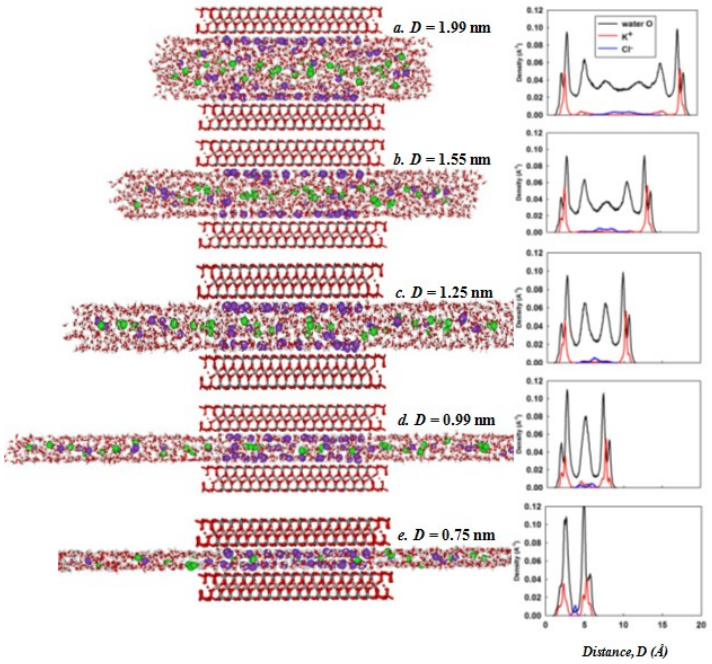

Figure 3. *Hydration structure of 1M KCl electrolyte solution between 2 mica surfaces. K^+ ions are in dark pink and Cl^- co-ions are in green.*

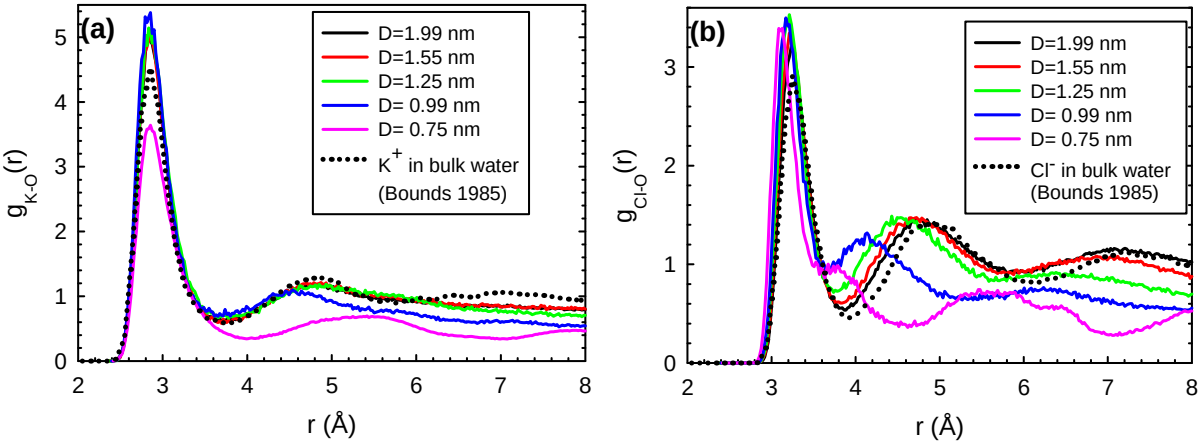

Figure 4. The variations of pair correlation functions of (a) K^+–water and (b) Cl^-–water in 1M KCl electrolyte solution under different degrees of confinement.

3. Force oscillation and phase transition of simple fluids under confinement

Unlike in polar aqueous electrolytes, when two molecularly smooth surfaces approach each other in a nonpolar simple liquid [such as liquid argon, cyclohexane, or octamethyl-cyclotetrasiloxane (OMCTS)] to nanometers distance, liquid films are squeezed out and solvation force oscillations between the surfaces are often observed. This phenomenon was reported early in 1980s by Horn & Israelachvili (*J. Chem. Phys.* 1981); Christenson, (*J. Chem. Phys.*1983), and had raised fundamental interests due to the inherent complexity of the structure and dynamics involved in nanoconfined fluids. Theories predicted that the layering transition of confined nonpolar fluids follows a nucleation-growth mechanism during dynamic squeeze out. However, what is really happening that accompanies force oscillations in surface force measurements, and in particular, how the confined fluid undergoes liquid-to-solid phase transition (Klein & Kumacheva, *Science* (1995)], is still not well understood.

In LVMD simulations, a simple driving spring model was applied to mimic the force measurement in surface force experiments. The force-distance profiles obtained from simulations (Fig. 5a) are strikingly similar to those in surface force measurements (see Fig. 5b). Detailed LVMD simulations showed that the force oscillation was accompanied by an abrupt liquid-to-solid phase transition, beginning from a slightly larger distance at D ~ 2.6 nm (point A in Fig. 5a). The three panels in Fig. 6 show that at this critical distance, the nucleation of layered structure starts at the central region. It is seen find that this layered structure grows and propagates outward to the edges of the central wall within 1.04 ns. To demonstrate that this layered structure is indeed in a solid phase, we further applied a shear force along the lateral direction to the film at point B, corresponding to a slightly higher pressure (~ 60 MPa) at D = 2.5 nm. We found that the layered structure can sustain a finite shear stress (~ 6 MPa) after an initial pulling of 1 Å, while the liquid phase before solidification (point *a* in Fig. 5a) cannot support any static shear stress with the same initial pulling. For subsequent $n = 6 - 2$ layered structures, further compression before $n \rightarrow n - 1$ layer transition always finds more ordered solid phase under higher pressures.

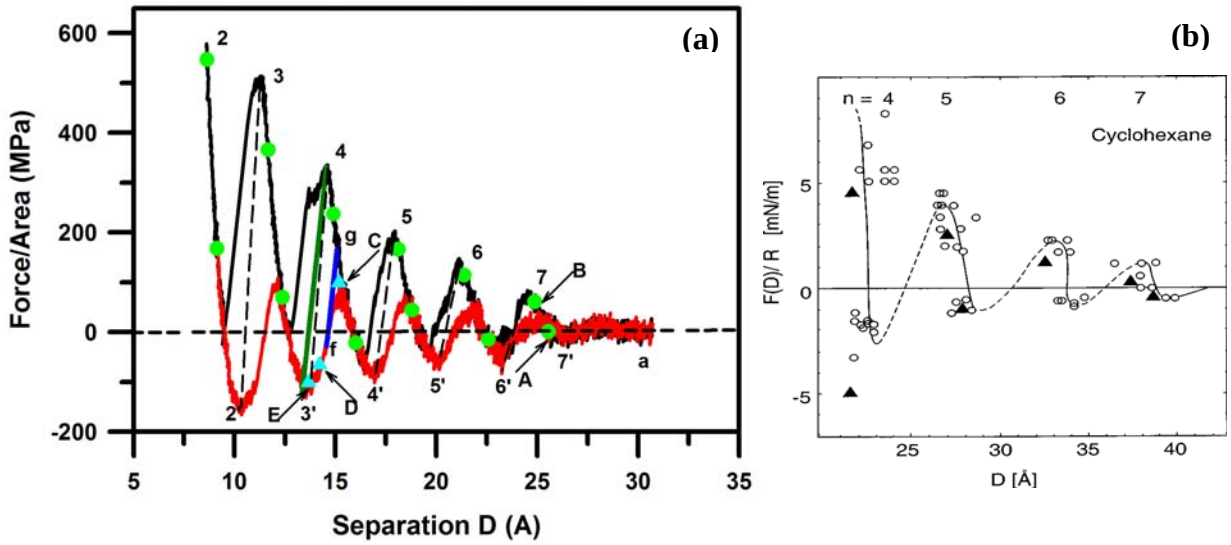

Figure 5. Solvation force oscillations between two crystalline walls in an argon droplet. (a) Force-distance profiles between two solid surfaces in argon during normal approach (black solid line) and retraction (red solid line). The number n and n' of monolayers corresponding to each force maximum and minimum. The solid circles A, B, etc. and solid triangles E, D, and C represent static forces during normal approach and retraction, respectively. The dashed lines show unstable $n \rightarrow n$ - 1 transition regions during normal approach, in which the force gradient $|\partial F/\partial D| > k_y$. The lines *4-3'* and *f-g* correspond to force relaxations of unstable transitions of $4 \rightarrow 3$ and $3 \rightarrow 4$, respectively. **(b)** Solvation force oscillations of cyclohexane confined between two mica surfaces. This experimental force profile curve was measured by Jacob Klein's group (*Science* 1995).

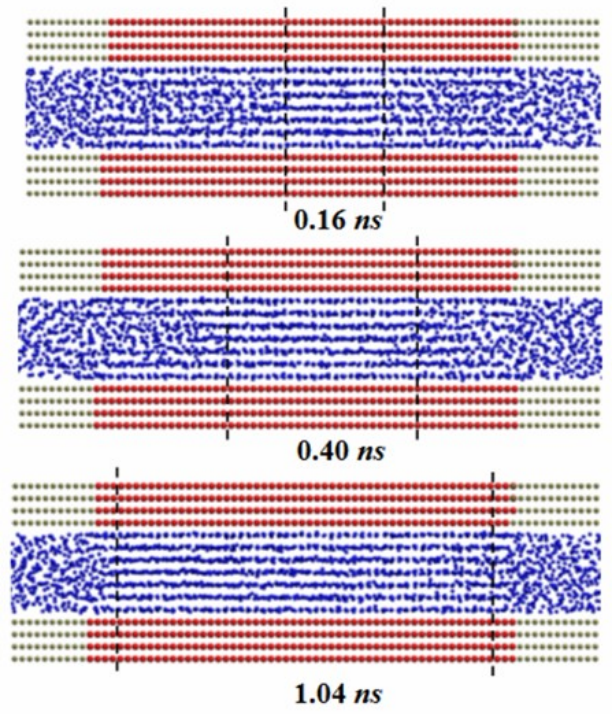

Figure 6. Liquid-to-solid phase transition at n = 7. At a critical distance of 2.6 nm, nucleation of solid phase starts at the central region. This solid phase grows and propagates outward to the edges of the central wall within 1.04 ns.

Further LVMD simulations on the realistic cyclohexane-mica contact show the very similar force oscillation and phase transition behavior of liquid cyclohexane confined between mica surfaces. We find that the first-order liquid-to-solid phase transition proceeds at 4-5 monolayers between the two mica surfaces (Fig. 7a). The force-distance profiles obtained from simulations (Fig. 7b) are very similar to those in surface force measurements (Fig. 5b).

(a)

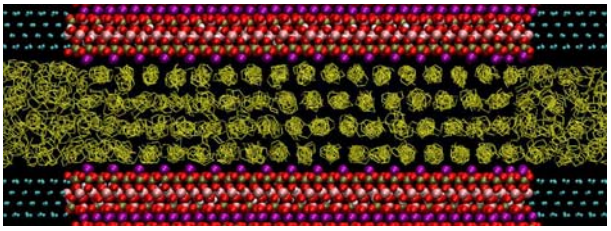

(b)

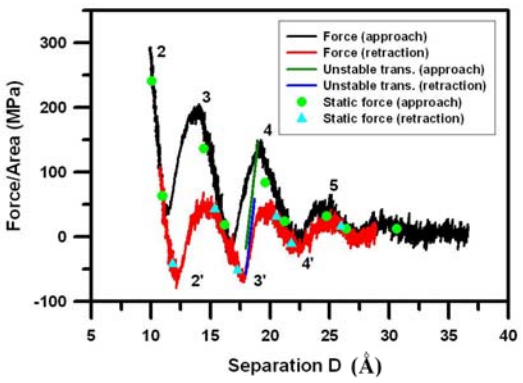

Figure 7. (a) Solidified structure of cyclohexane liquids confined to $n = 4$ monolayers**. (b)** Force-distance profiles between two mica surfaces in cyclohexane during normal approach (black solid line) and retraction (red solid line). The number n and n' of monolayers corresponding to each force maximum and minimum. The solid circles and solid triangles represent static forces during normal approach and retraction, respectively. The green and blue lines correspond to force relaxations of unstable transitions of $4 \rightarrow 3$ and $3 \rightarrow 4$, respectively.

In 2010, Cummings and co-workers published an invited Perspectives article in the AIChE Journal, the flagship journal of the American Institute of Chemical Engineers, reviewing the long-running experimental controversy concerning phase transitions under nanoconfinement, and his group's decade-long simulation studies demonstrating the existence of phase transitions under nanoconfinement [Cummings, P., Docherty, H., Iacovella, C., and Singh, J. (2010). Phase Transitions in Nanoconfined Fluids: The Evidence from Simulation and Theory. *AIChE Journal*, *56*(4), 842–848]. This Perspective article was featured on the cover of AIChE Journal (see Fig. 8).

Figure 8. Cover page image featuring the work in Cummings' group.

4. Stick-slip friction and energy dissipation in boundary lubrication

Stick-slip motion of solids over each other in boundary lubrication is often observed in our daily lives. This phenomenon has been studied through well-controlled surface force experiments and molecular simulations. One generic conclusion is, for simple nonpolar fluids, stick-slip friction is associated with the solidification and shear melting of the confined film. However, one cannot directly observe shear melting in surface force measurements, except computer simulations. A phenomenological analysis showed that most of the friction dissipation occurred by the viscous heating of the shear-melted film during this slip. Through LVMD simulation we demonstrate that shear melting is not necessarily a pathway for the energy dissipation during the slip. Instead, boundary slips at the wall-fluid interfaces and interlayer slips within the film are the ways of energy dissipation. We find that during the slip, the crystalline structure of the solidified film can be well maintained.

A simple driving spring model in the lateral direction is used to simulate sliding friction (Fig. 8A). Stick-slip friction force and the motions of the displacement of the top wall, as well as the slips of four monolayers in the solidified film are shown in Fig. 10B and 10C, respectively. When the maximum static friction force (the yield point) of the film is exceeded, it is seen that instead of shear melting, the solidified film undergoes boundary slips at the wall-film interface, and interlayer slips within the film. The slip usually completes within ~ 20 ps, with a jump of 1 - 3 Å. Figure 10D shows the in-plane structure factor q (based on the hexagonal close-packed (hcp) crystalline structure) of each monolayer versus fluctuates around 0.9, further demonstrating the solidlike structure of the film during the stick-slip motion. During the slips, q of each monolayer slight drops to 0.5 ~ 0.7. This is due to the distorted hcp structure at the instant of slip (see the inset panel *b* in Fig. 10D).

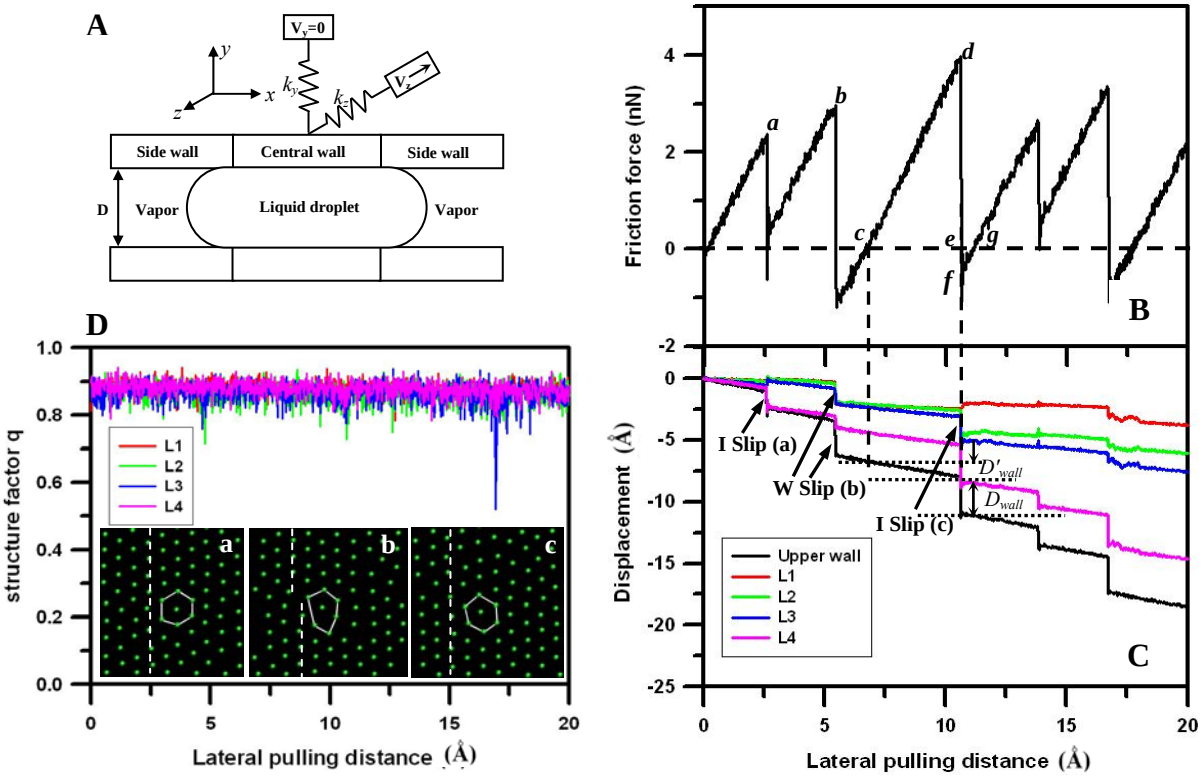

Figure 10. A. Schematic of the LVMD simulation geometry. **B.** Variation of the stick-slip friction force as a function of lateral pulling distance at a driving velocity v = 0.01 m/s. **C,** Displacements of the top wall and the four monolayers in the solidified film relative to the bottom fixed wall. Here, the I-slip and W-slip refer to the interlayer and wall slips, respectively, and D'_{wall} and D_{wall} are the wall displacements during the stick and slip in the *c-d-e* stick-slip cycle. **D.** The variations of the in-plane structure factors of L1-L4 monolayers during the stick-slip motion. The broken dashed line in the inset panel b shows the lattice mismatch due to the distorted hcp structure of argon molecules in the slip. The three snapshots show a typical series of molecular configurations for the L2 monolayer before, during and after the slip. In the mean time, we also observed interlayer atomic jumps during the slip, which are associated with the vacancy diffusion within the film[16].

The mechanism of energy dissipation during stick-slip friction is analyzed below. Before the slip proceeds, the total external work W_{ext}, done by the driving block to the molecular system is stored in the form of the spring elastic energy ΔE_{spr} and the potential energy increase ΔE_p of the solidified film. For a typical stick-slip motion of the top wall (c-d-e-f-g in Fig. 10B), Fig. 11A shows the variations of the spring force and the wall slip displacement versus time in a single slip event (d-e-f in Fig. 10B). The two curves show that energy dissipation proceeds in two stages: the friction dissipation during the slip and the residual momentum loss of the top wall in the remaining ringing vibrations. These two processes are remarkably similar to those in the surface force measurement and phenomenological analyses (Klein, *Phys. Rev. Lett.* 2006). Figure 11B shows the very detailed slip behavior of the top wall in a much smaller time scale. The friction force (the spring force measured in the surface force experiments), F_z, and the surface force, W_z experienced by the top wall are shown in the inset of Fig. 11B. Through the detailed analysis of the energy dissipation, we found that friction dissipation in boundary lubrication is the one where, during the stick, elastic energy is stored both in the driving spring as well as in the confined solidified film, with the former accounting for 70% of the stored energy. During the slip, more than 90% of spring energy ΔW_{spr}, or 60% of the total elastic energy is dissipated as friction heating due to interlayer slips and wall slips. The remaining 40% energy is dissipated as potential energy release in the solidified film and momentum loss of the wall during the subsequent mechanical oscillations at the instant of new stick. This part of energy dissipation is much larger than the one based on the shear melting model (Thompson and Robbins, *Science* 1990; Klein, *Phys. Rev. Lett.* 2006).

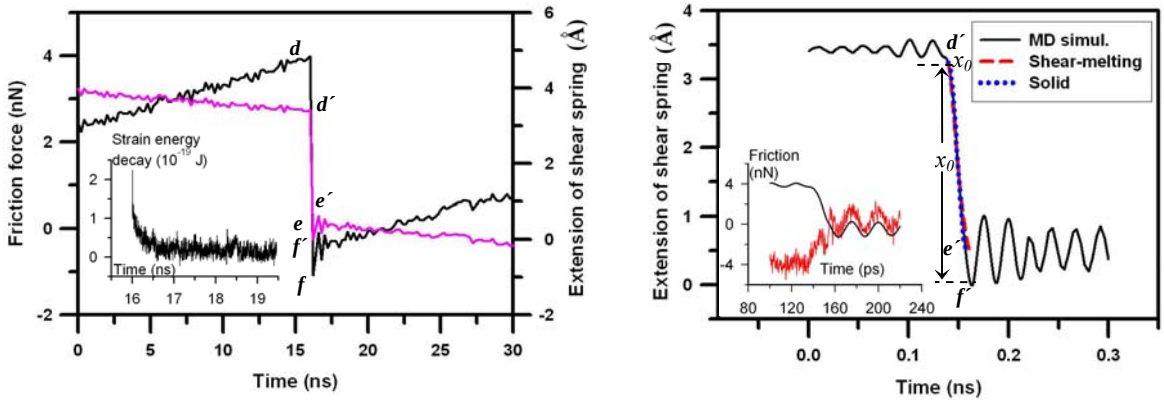

Figure 11. A. Shear force (black line) and shear displacement of top wall (pink line) for a typical stick-slip cycle under normal load of 7.45 nN. The inset shows the decaying of potential energy in the solidified film after slip. **B.** Slip of the top wall at magnified time scale. The blue dotted line corresponds to the predicted variation of $x(t)$ given by the solid friction model, while the red dashed line corresponds to the shear-melting model. The inset shows the exact variations of the spring force (black) and surface force (red) during the short stick-slip-ringing period. Points *d'*, *e'* and *f'* correspond to the maximum extension, zero extension, and maximum compression of the driving spring, respectively.

Computational Codes Used in the Project:

(1) In-house water-mica-cation (MWC) FORTRAN 90 for nanoconfined electrolyte system;
(2) LAMMPS (Large-scale Atomic/Molecular Massively Parallel Simulator) community code, developed by Plimpton et al. from the Sandia National Laboratories.

Personnel Supported:

Yongsheng Leng, Assistant Professor, Department of Mechanical & Aerospace Engineering, George Washington University

Dr. Yajie Lei, Postdoctoral Scientist, Department of Mechanical & Aerospace Engineering, George Washington University

Peter T. Cummings: John R. Hall Professor of Chemical Engineering, Department of Chemical and Biomolecular Engineering, Vanderbilt University

Hugh Docherty, Postdoctoral Research Associate, Department of Chemical and Biomolecular Engineering, Vanderbilt University

Publications:

1. Leng, Y. S. "Hydration force between mica surfaces in aqueous KCl electrolyte solution," (submitted).
2. Lei, Y. J. and Leng, Y. S., "Slick-slip Friction and Energy Dissipation in Boundary Lubrication", *Physical Review Letters* **107,** 147801 (2011).
3. Lei, Y. J. and Leng, Y. S., "Molecular dynamics simulations on the phase transition of simple nonpolar fluids under nanometer confinement", *Proceedings of the Institution of Mechanical Engineers, Part N, Journal of Nanoengineering and Nanosystems*, **224**, 69 (2011).
4. Lei, Y. J. and Leng, Y. S., "Force oscillation and phase transition of simple fluids under confinement", *Physical Review E* **82,** 040501 (*Rapid Communications*) (2010).
5. Leng, Y. S., Lei, Y. J., and Cummings, P. T., "Comparative studies on the structure and diffusion dynamics of aqueous and nonpolar liquid films under

nanometers confinement" *Modeling and Simulation in Materials Science and Engineering* ***18***, 034007 (2010).

6. Leng, Y. S. "Hydration force and dynamic squeeze out of hydration water under subnanometer confinement," *Journal of Physics: Condensed Matter* **20**, 354017(2008).

7. Cummings, P., Docherty, H., Iacovella, C., and Singh, J. (2010). Phase Transitions in Nanoconfined Fluids: The Evidence from Simulation and Theory. *AIChE Journal*, *56*(4), 842–848.